Highlights of Recent Fusion Materials Tungsten Research

R.J. Kurtz (PNNL)

Contributors: N.M. Ghoniem (UCLA), J. Marian (LLNL), G.R. Odette (UCSB), R.E. Stoller (ORNL), and B.D. Wirth (UT)

Presented at:
MASCO/PFC Joint Session on Tungsten Research
Oak Ridge National Laboratory
Oak Ridge, TN
August 10, 2011

Work supported by the U.S. Department of Energy, Office of Fusion Energy Sciences

Pacific Northwest
NATIONAL LABORATORY

Plasma Facing Materials Must Tolerate Extreme Heat, Neutron & Particle Fluxes

Baldwin, Nishijima, Doerner, et. al, courtesy of Center for Energy Research, UCSD, *La Jolla, CA*

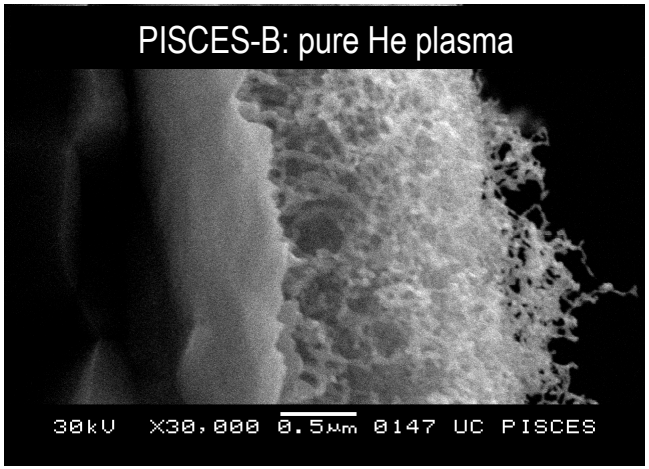

M. Rieth, A. Hoffmann, HHFC, 2008

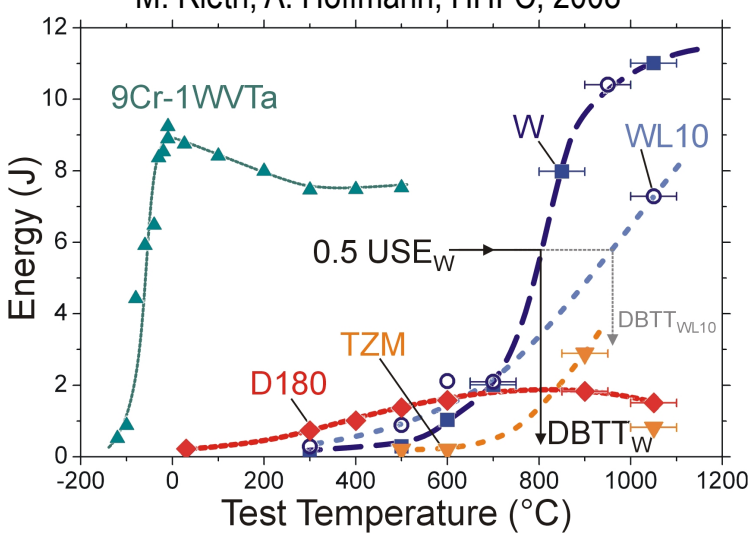

- Typical materials considered for PFM include graphite, beryllium and tungsten.
- Tungsten alloys leading candidates as divertor structural materials due to their excellent thermo-physical properties.
- However, critical issues need to be addressed:
  - ❖Creep strength
  - ❖Fracture toughness (DBTT)
  - ❖Microstructural stability (Recrystallization)
  - ❖Low & high cycle fatigue
  - ❖Oxidation resistance
  - ❖Effects of neutron irradiation (hardening & embrittlement, composition changes, He, H)
- A computational and experimental effort to explore ways to improve the properties of tungsten alloys was recently begun.

Research Tasks

I. Computational Modeling
   - Ductilizing solutes, dislocation nucleation & mobility, grain boundary chemistry & cohesion, near surface He effects

II. Test Methods & Characterization Protocols
   - Deformation & fracture, thermal creep

III. Fundamental Studies of Cleavage Fracture

IV. Intergranular Fracture & Grain Boundary Embrittlement

V. Alloy Development
   - Solute softening, nanostructured alloys, composites & ductile phase toughening

VI. Processing & Joining Technology

VII. Irradiation Effects

VIII. Surface & Dimensional Stability

Mechanical Properties of W Alloys

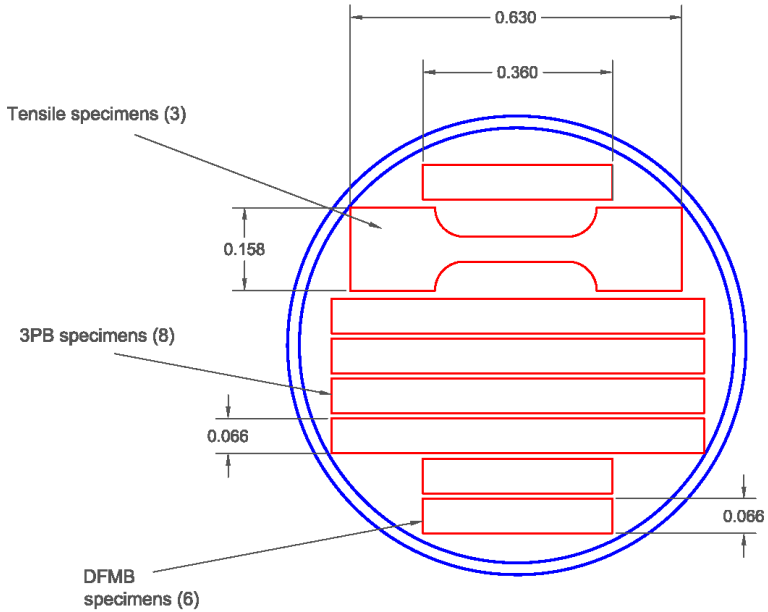

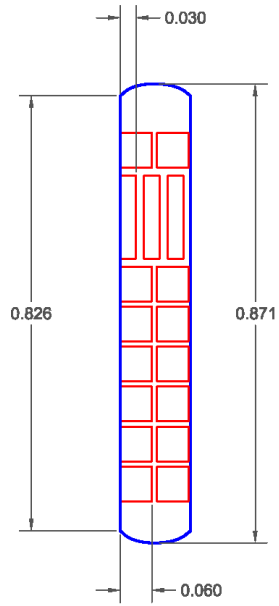

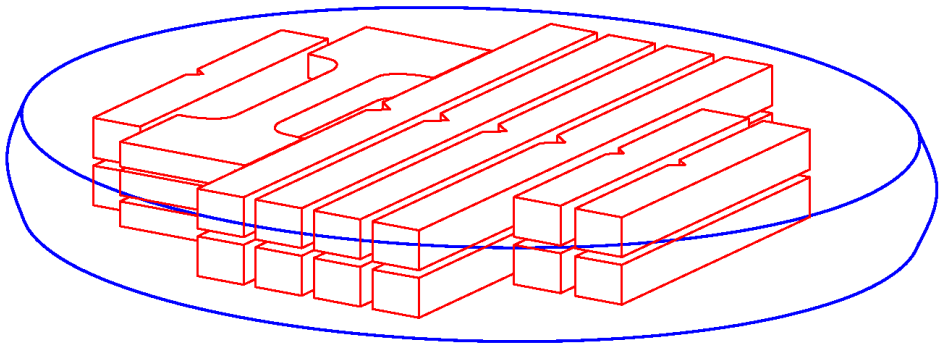

Layout of W-1.1TiC Disk
Drawing number: NMST - 072710
Drawn by: Eric Manneschmidt

- Material obtained from Prof. Hiroaki Kurishita, Tohoku University, Oarai
- Specimens currently being fabricated

Materials Obtained from KIT (M.Rieth)

1) W and WL10 (W with 1 wt. % La_2O_3) rods, diameter 8 mm, commercial standard weld electrodes, produced by sintering and hot rolling. Final fabrication process: surface grinding.
2) WTa5 (W-5wt.%Ta), WTa1 (W-1wt.%Ta), round blanks, fabricated by sintering and forging, deformation degree is about 80%.
3) WUHP (ultra high purity, as far as industrially possible), same product and fabrication as 2)
4) WVM (tungsten doped with K, for lamp industry), same production and fabrication as 2)

All materials were produced by PLANSEE, therefore the exact fabrication details like sintering parameters or rolling/forging details are not known.

Re effects – Mo-Re model system

- Leftover from space program will be used to perform fracture toughness and mechanical properties of W-25Re alloy
- Mo-15Re alloy has been melted and ready to be extruded and rolled
- Mo-25Re alloy is about to be melted
- Mo-20Re and Mo-35Re are in preparation

Modeling of dislocations in W-M binary alloys

<111>/2 dislocation quadrupole

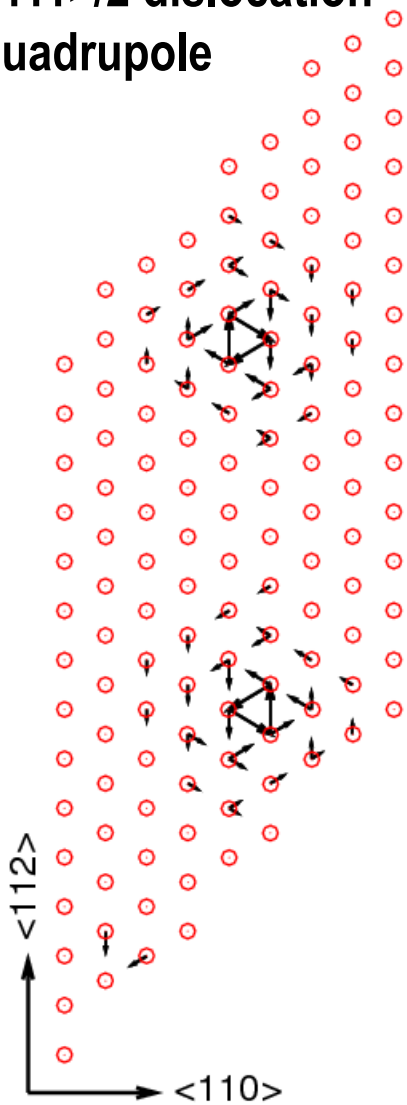

Quadrupole of screw dislocations can be reduced to pair of dislocations in the cell with translation vectors:

$$\vec{h}_1 = (9\vec{u}_1 + 5\vec{u}_2 + \vec{u}_3)/2$$

$$\vec{h}_2 = 5\vec{u}_2$$

$$\vec{h}_3 = \vec{u}_3$$

where

$$\vec{u}_1 = <110>$$

$$\vec{u}_2 = <112>$$

$$\vec{u}_3 = <111>/2$$

Quantum-espresso, ultra-soft pseudo-potential, PW91 xc,
8x2x1 k-points
135 atoms in the cell

Modification of easy core dislocation structure in W with alloying

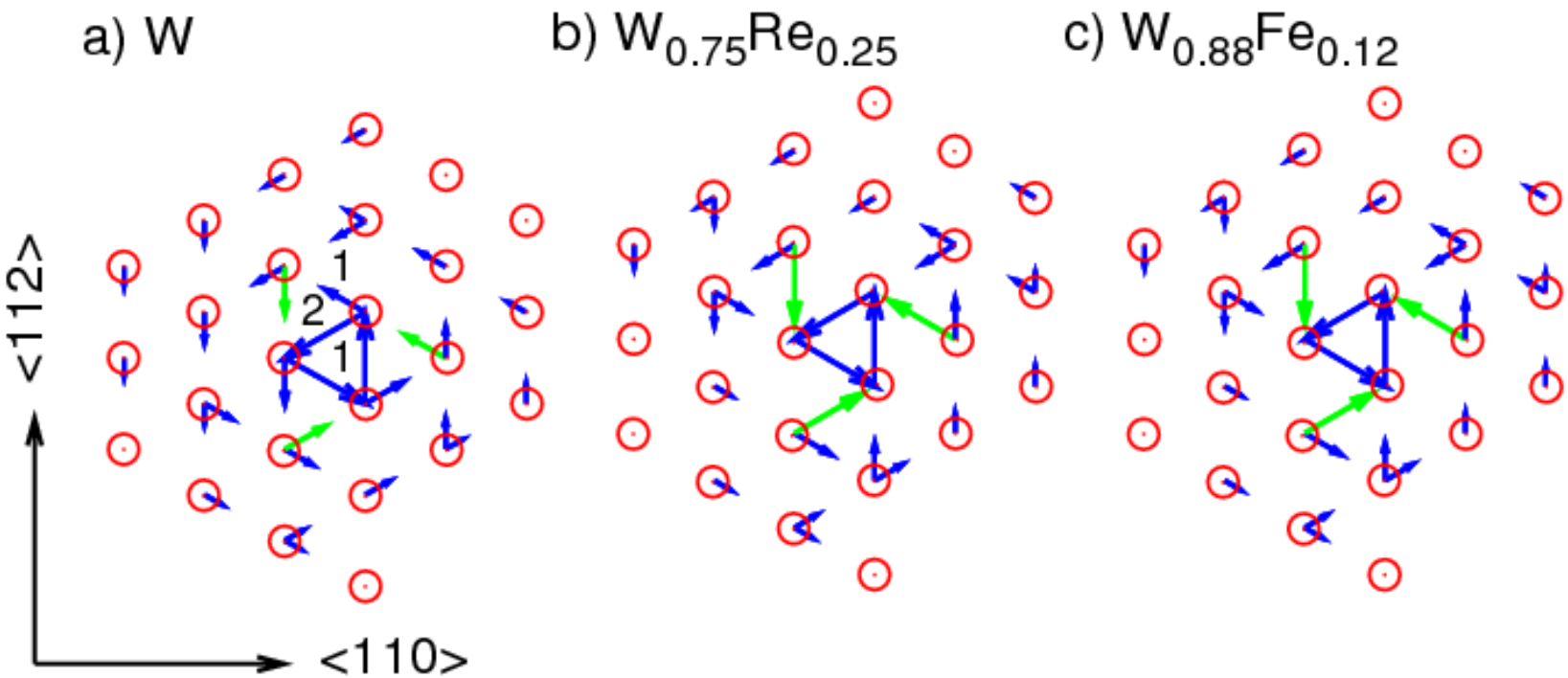

Non degenerate, symmetric

Degenerate, asymmetric

After alloying with Tm with larger number of valence electrons per atom

Peierls barrier calculation

Peierls barrier separates two easy core configuration

(Could correlate with Peierls stress and easy for calculations)

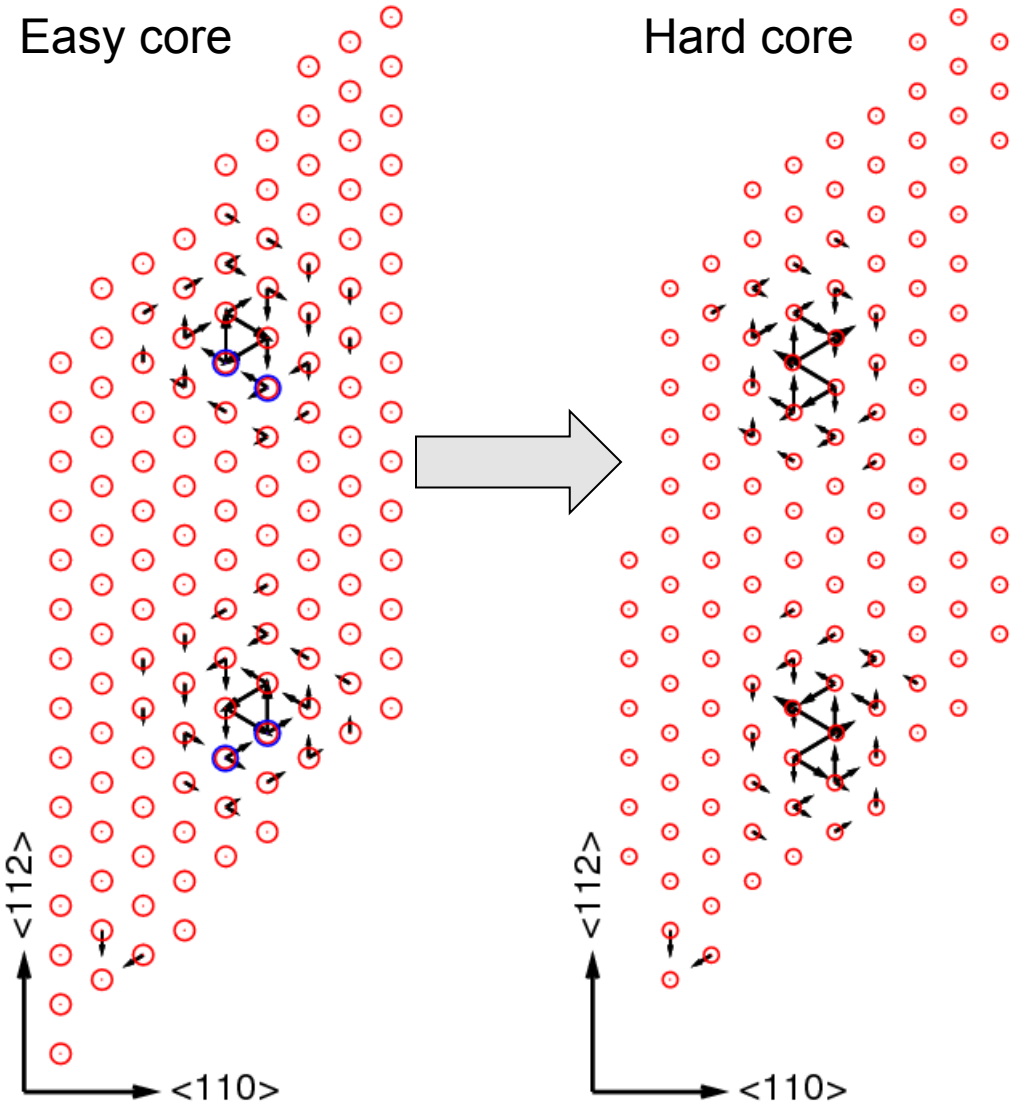

Reaction coordinate method used to calculate Peierls barrier.

Keep *z* position of atoms in columns shown by blue and relax all other atoms

$$z = x \cdot z_{\text{easy core}} + (1 - x) z_{\text{hard core}}$$

x-reaction coordinate

Peierls barriers in W_xTm_{1-x}

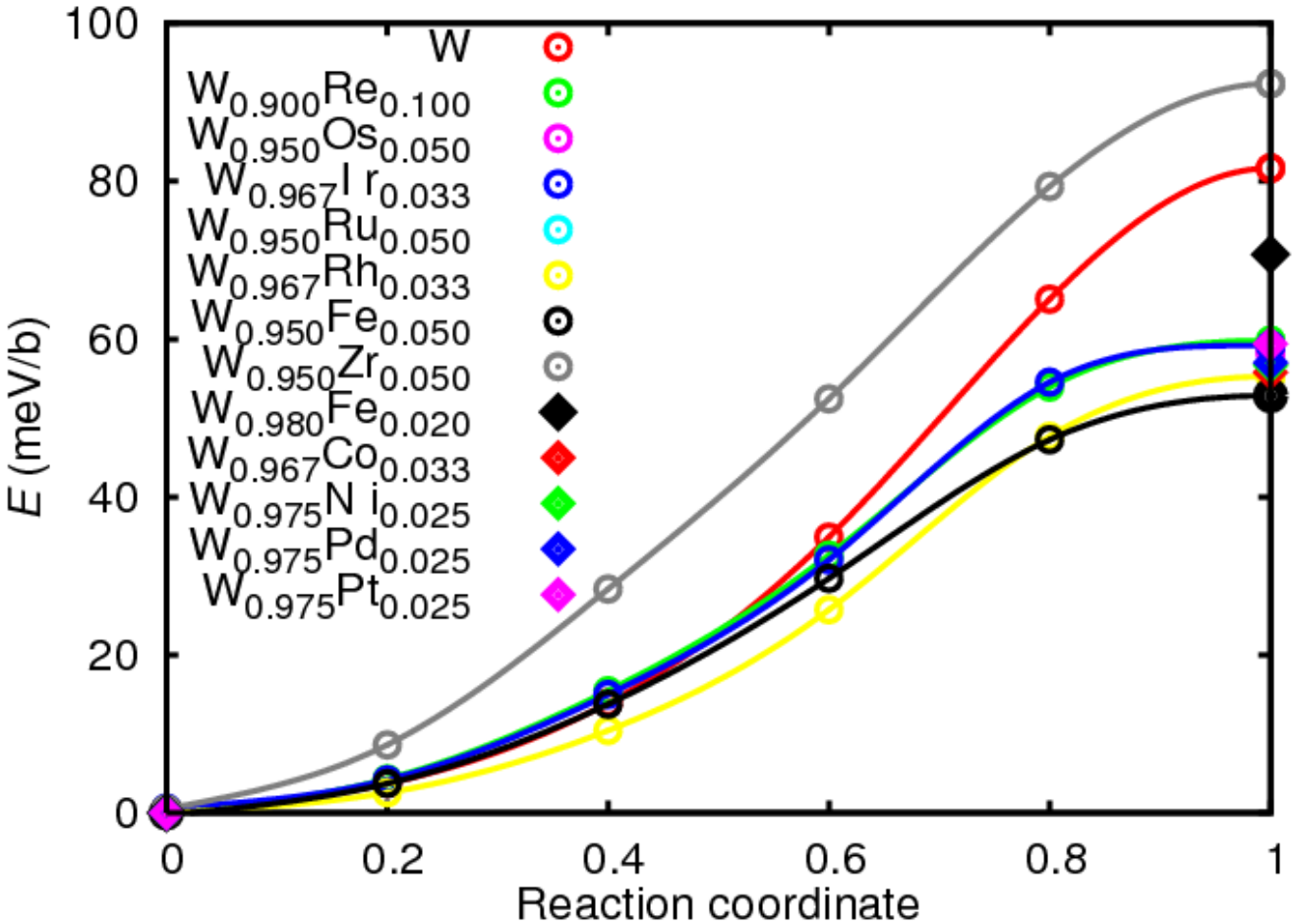

- Alloying with Tm with larger amount of valence electrons (VIIIA group) reduces Peierls barrier.
- Value of Peierls barrier reduction equal for alloys with the same averaged number of electrons per atom.

W-W potential development

- Previous work included modifying Ackland-Thetford Finnis-Sinclair (FS) type N-body potential
- Currently trying to improve Tersoff-type bond order potential (BOP)
  - BOP angular bonding well suited for hydrogen
  - Existing potentials for W-C-Be-H (Juslin & Nordlund)
  - ~5 times slower than FS/EAM
  - Potential contains 11 parameters, making fitting challenging

$$E = \sum_{i>j} f_{ij} \left[V_R^{ij}(r_{ij}) - \bar{b}_{ij} V_A^{ij}(r_{ij}) \right]$$

$$b_{ij} = \left(1 + \sum_{k(\neq i,j)} f_{ik}(r_{ik}) g_{ik}(\theta_{ijk}) e^{2\mu_{ik}(r_{ij} - r_{ik})} \right)^{-1/2}$$

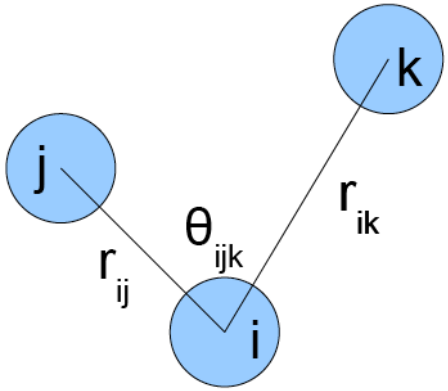

Existing W Tersoff potentials

- Juslin-Erhart 2005:
  - Bad point defects, low T_{melt}
  - Does work with existing W-C-Be-H potentials

- Ahlgren 2009:
  - Bad elastic properties, high T_{melt}
  - Long cutoff (incl. 3rd nn → ~3-4 times slower than 2nd nn cutoff BOP)

- Li 2011
  - Phases besides BCC more stable (structural instability during MD)
  - Long cutoff (incl. 3rd nn → ~3-4 times slower than 2nd nn cutoff BOP)
  - W-H potential appears to have errors (interstitial properties do not reproduce paper)

New (& Improved?) W Tersoff potentials

- An example of fit ‘work in progress’ among hundreds of fitting trials (New Juslin)

	Target	Jus	Ahl	Li	New Jus
B [GPa]	308 - 320	308	215	307	275
c11	500 - 550	542	444	515	466
c12	199 - 207	191	128	203	179
c44	151 - 160	162	134	162	184
$E_{f,vac}$ [eV]	3.6, 3 - 3.9	1.68	3.75	3.52	2.7
$E_{b,divac}$	-0.05 – 0.1 (?)	0.35	0.66	0.62	0.42
$E_{f,db110}$	9.8 - 10.3	8.77	10.5	9.53	9.58
$E_{f,db111}$	9.6 - 9.9	9.62	10.1	9.33	9.36
T_{melt} [K]	3695	2750	4550	4550	~3600
$\Delta E_{bcc\text{-}fcc}$ [eV]	0.2-0.4	0.34	0.25	0.2 (unst.)	0.2
D_0 [eV]	4.1 (?)	5.4	3.3	2.9	3.8
r_0 [A]	2.2 (?)	2.34	2.46	2.39	2.46

W-He-H potentials & small clusters

- Still finalizing W potential, but concurrently evaluating W-He-H
  - DFT data by Becquart & Domain
    [JNM 386-388 (2009) 109]

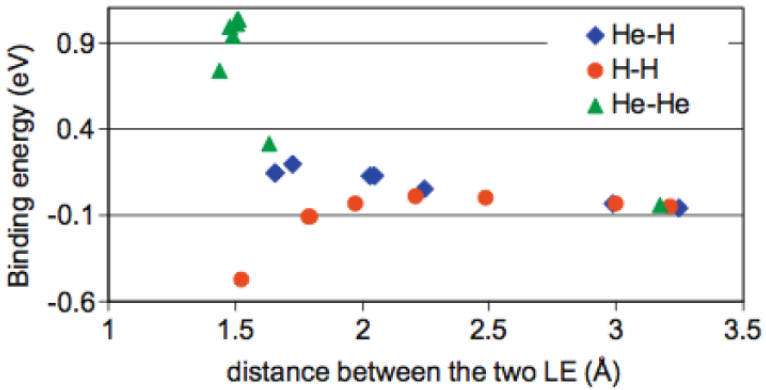

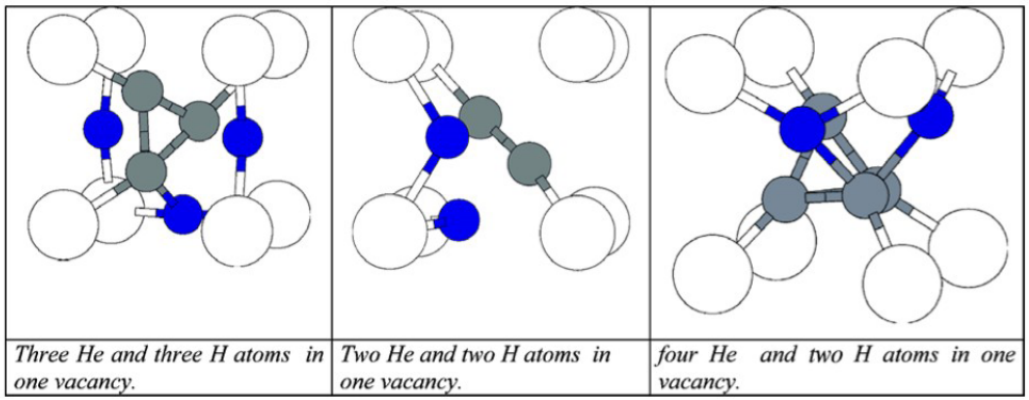

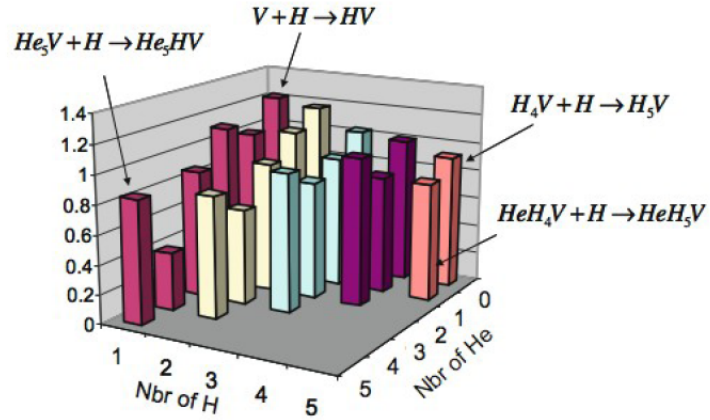

Fig. 3a. Binding energies (eV) for the reaction: $He_xH_yV + H \rightarrow He_xH_{y+1}V$.

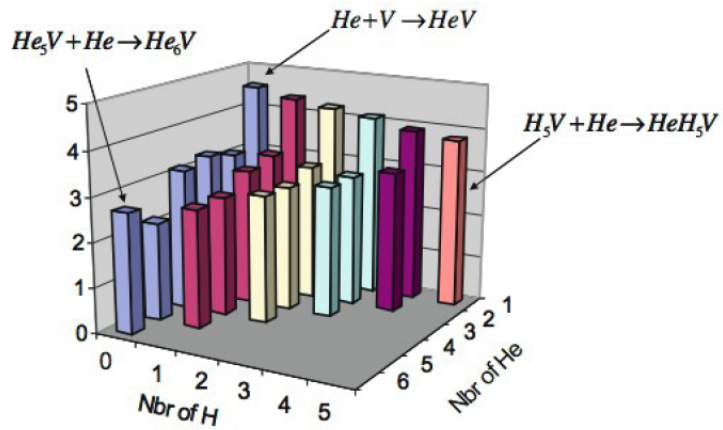

Fig. 3b. Binding energies (eV) for the reaction: $He_yH_xV + He \rightarrow He_{y+1}H_xV$.

½⟨111⟩{112} screw dislocation mobility in pure W

- We have systematically compared four W interatomic potentials:

Potential	Type	Core structure at 0K	Relative computational cost
Zhou	EAM	Dissociated	1
Juslin	BOP	Compact	7
CEA	EAM	Compact	1
MEAM	MEAM	Compact	10

- We study dislocation motion under applied shear stress in at high strain rates (~10^7 s^{-1})

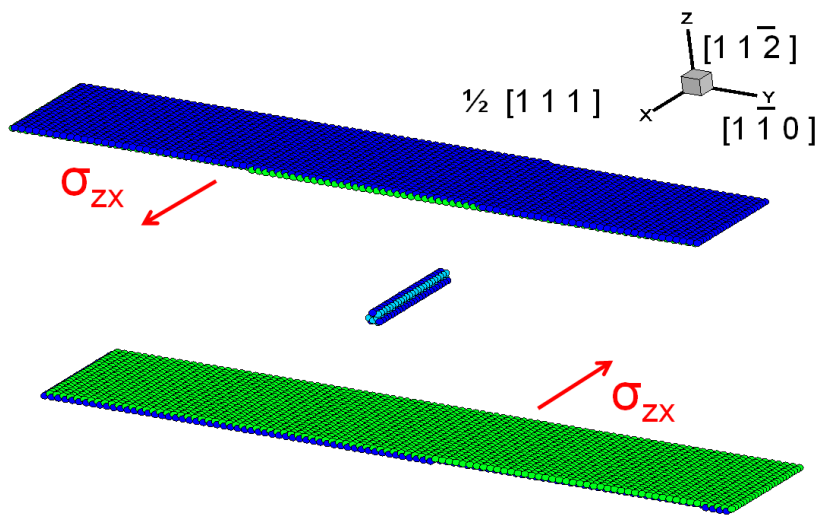

Boundary conditions are very important

- Stress must be gradually applied (from zero to desired value), e.g. as a linear time ramp. Otherwise large finite-size oscillations develop, resulting in a step-wise time-displacement response:

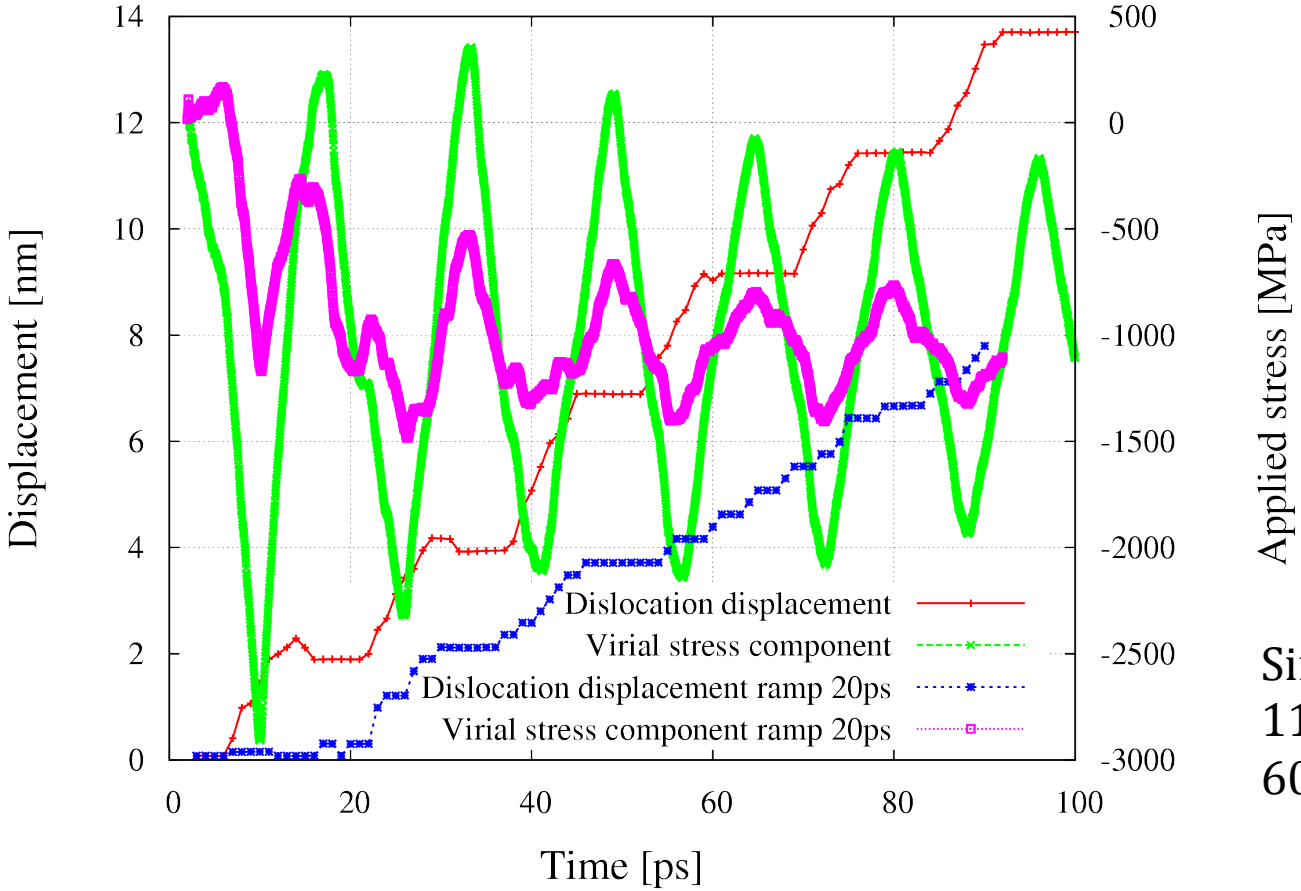

Simulation at 1100 MPa and 600K

Dislocation velocities as a function of stress and temperature

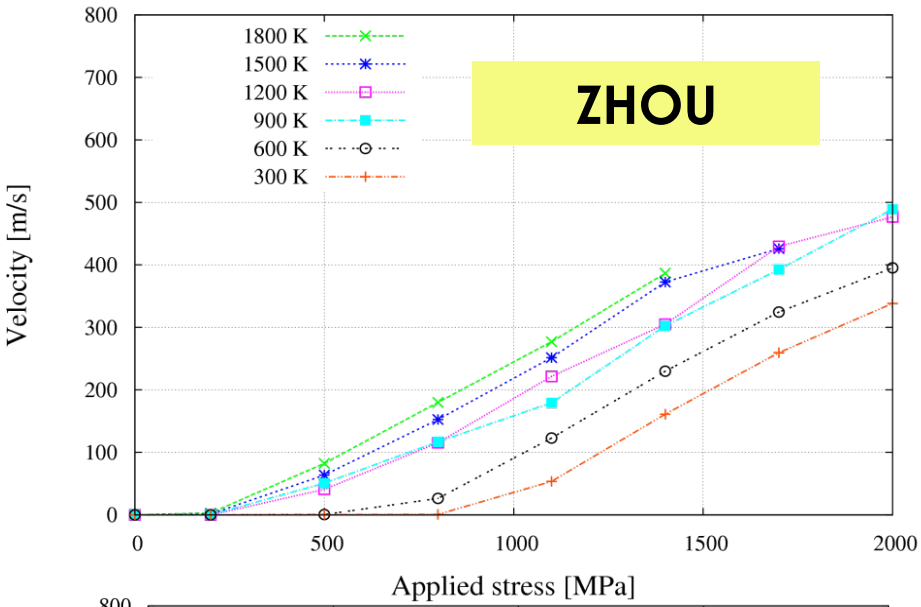

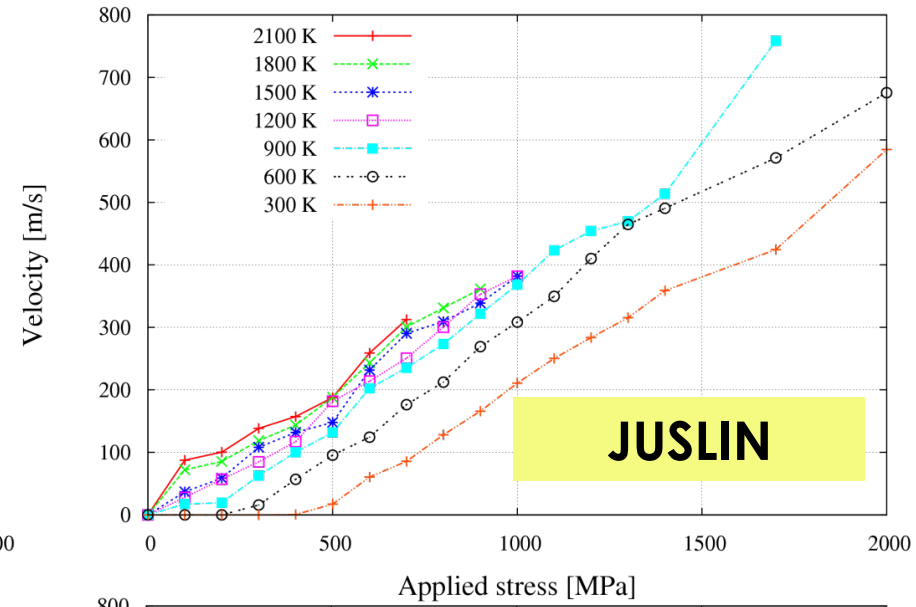

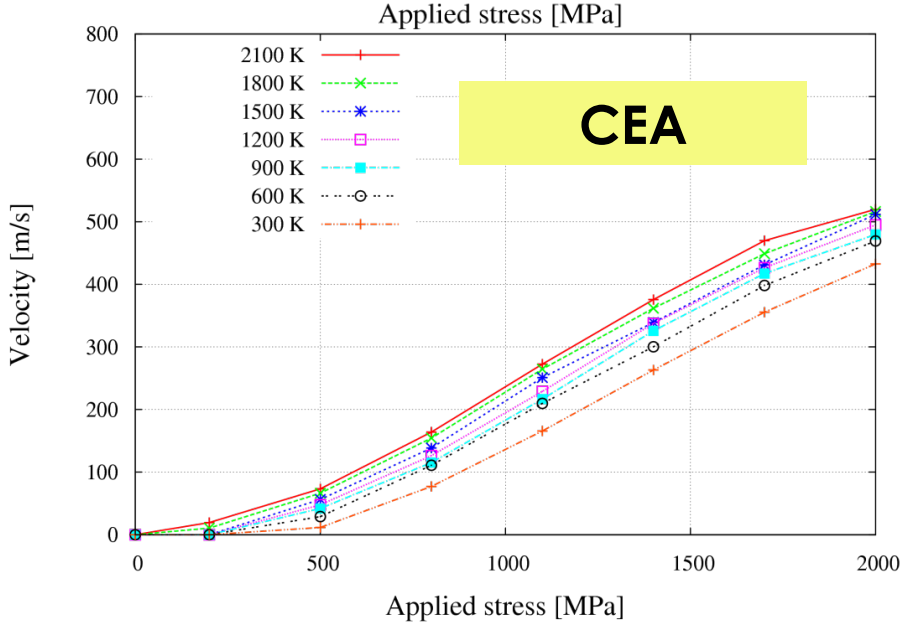

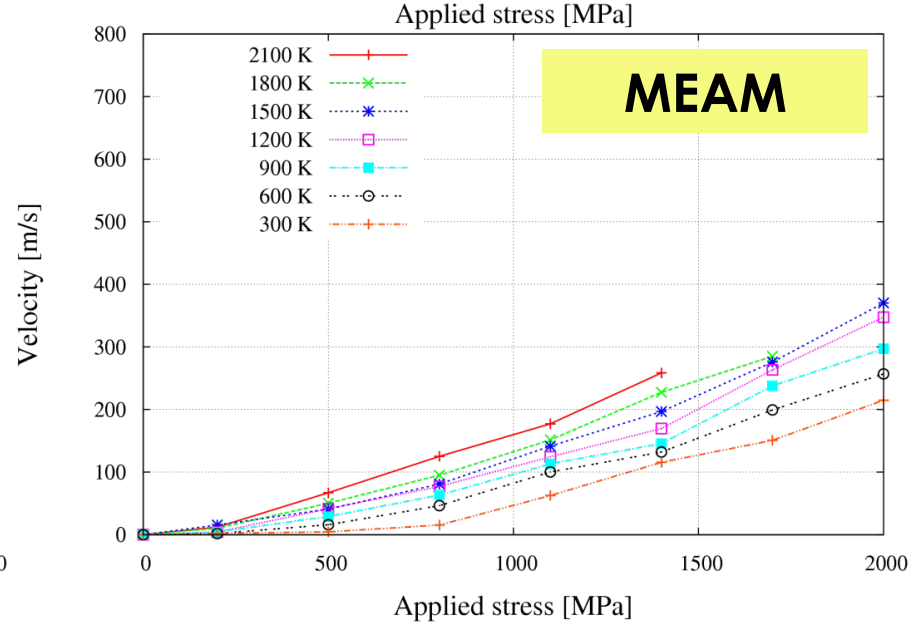

Comparison of potentials at different temperatures

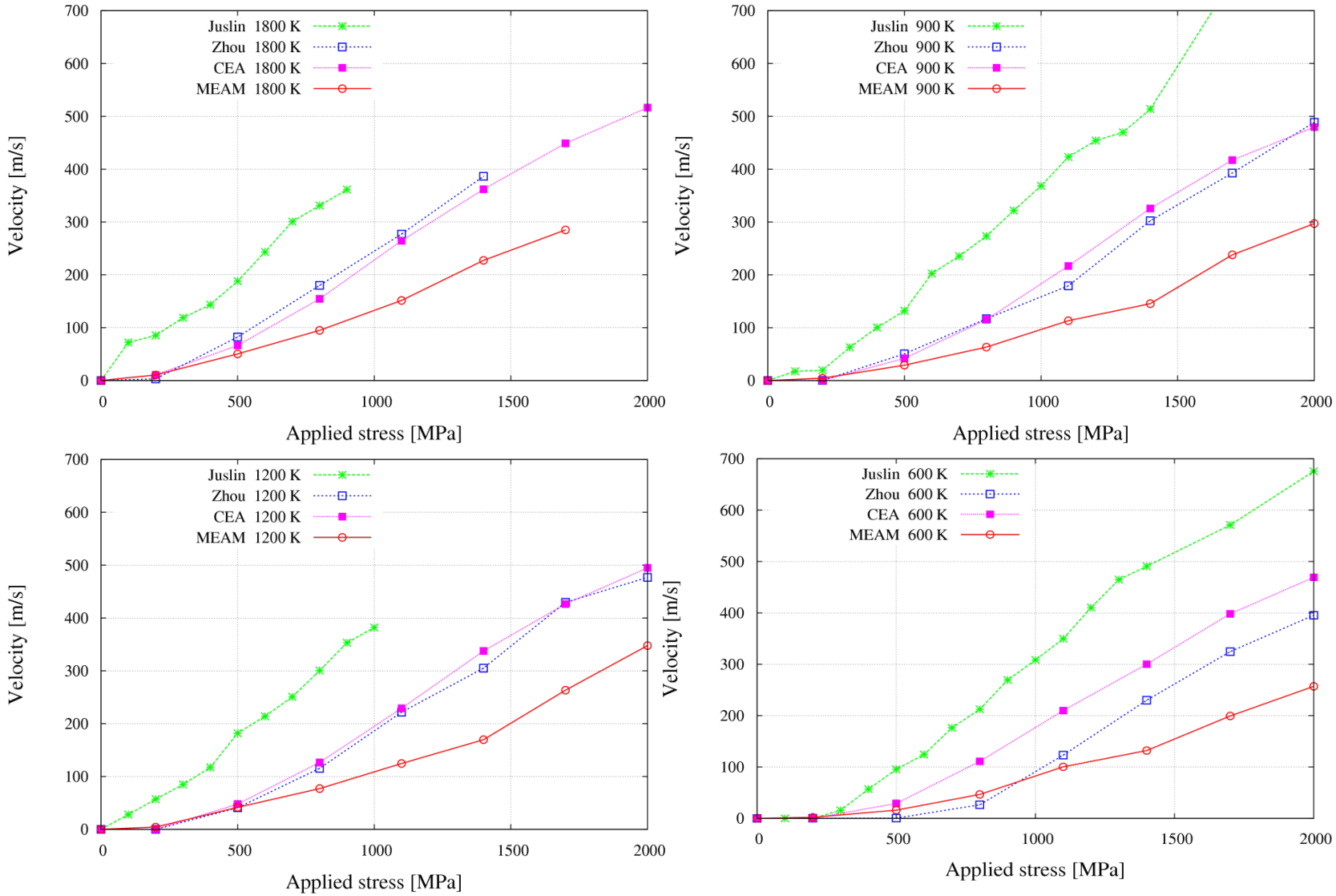

Dislocation dynamics modeling of edge-He bubble interaction (in collaboration with B Wirth, builds up on previous work by N Ghoniem)

- In quasistatic DD, interaction is controlled by mechanical equilibrium in *D*:

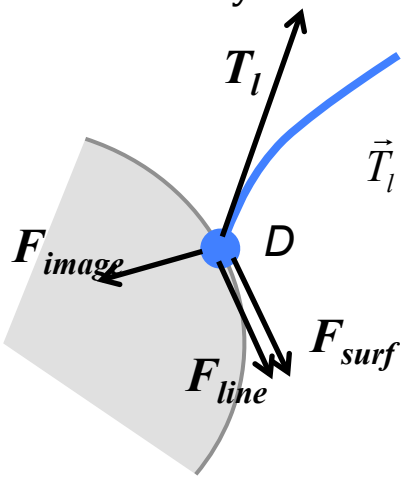

$$\vec{T}_l + \vec{F}_{line} + \vec{F}_{surf} + \vec{F}_{image} = \vec{0}$$

- A physically-based model that takes into account 'shearing' of small voids is proposed:

Atomic features → DD + Continuum mechanics

Contact interaction

1-Line energy reduction

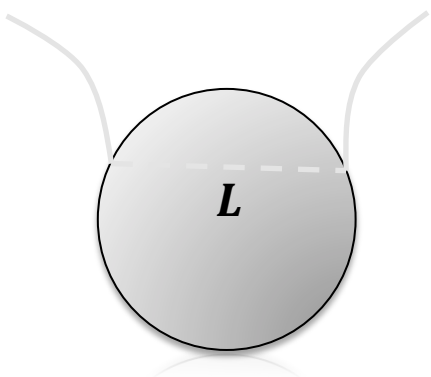

2-(110) Surface step

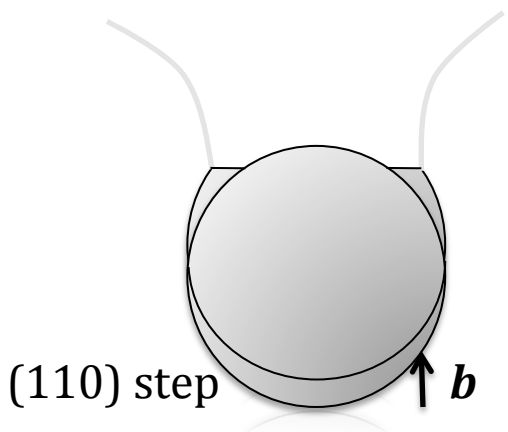

Remote interaction

3-Image stress / free surface

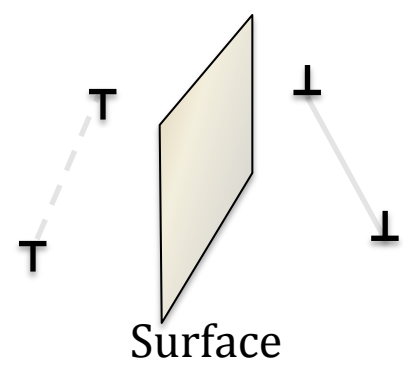

Tungsten Grain Boundary Energy:

Convergence Study

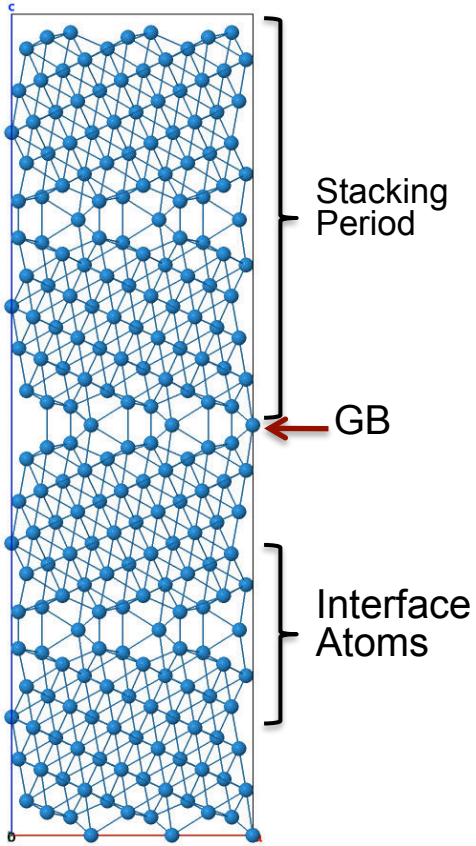

- Full periodic boundary conditions.
- Allow atoms and cell to relax with a simpler "zero force" tolerance than slab configuration.
- Need thick enough stacking period to minimize GB-GB interaction.

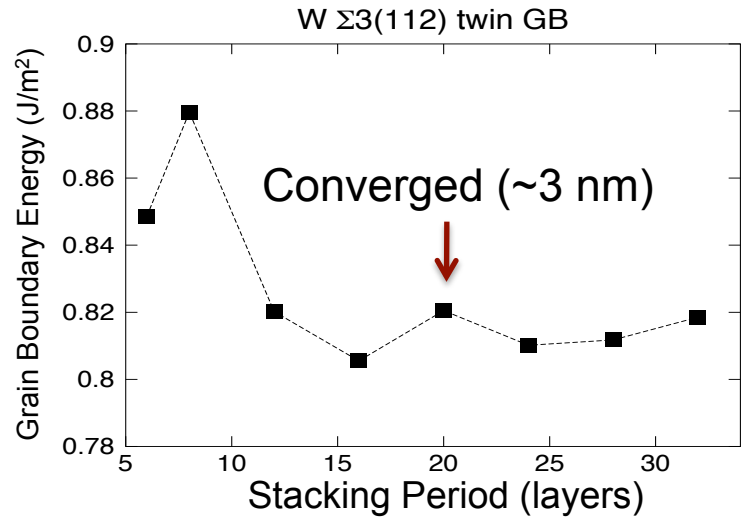

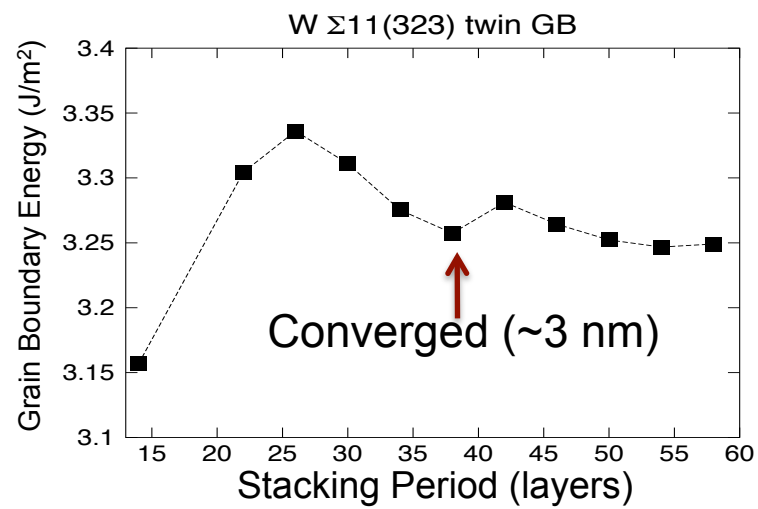

Σ27(525) GB will be simulated with layer thickness also ~3 nm

Effect of Interstitial Elements on W Grain Boundary Cohesive Energy

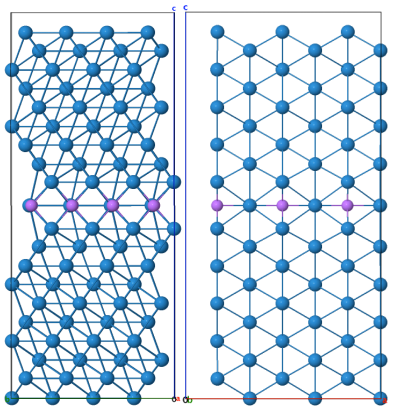

Impurity = 8.2 nm^{-2}

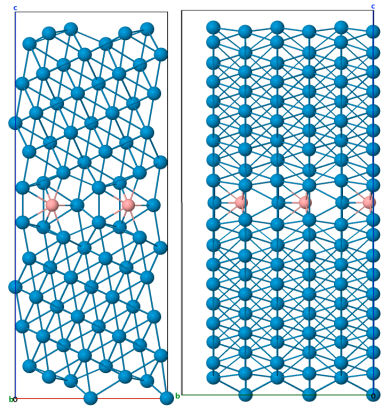

Impurity = 4.3 nm^{-2}

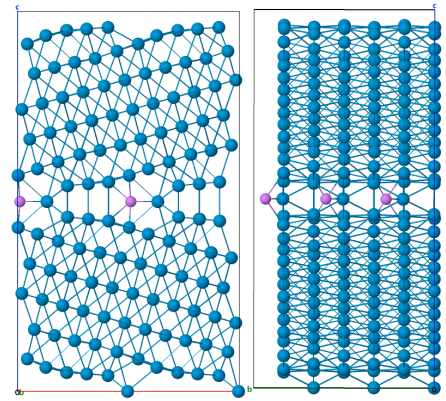

Impurity = 2.7 nm^{-2}

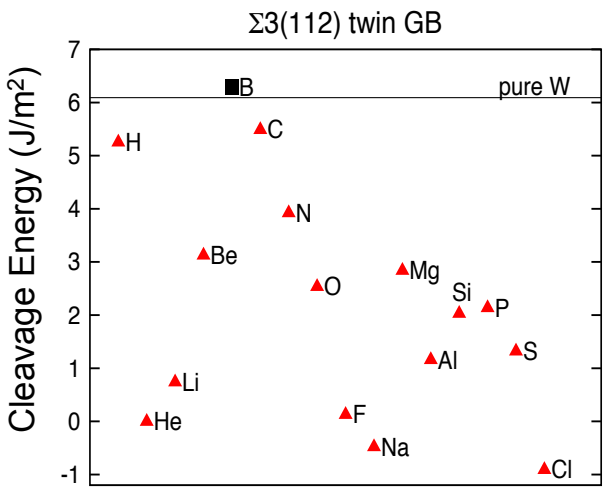

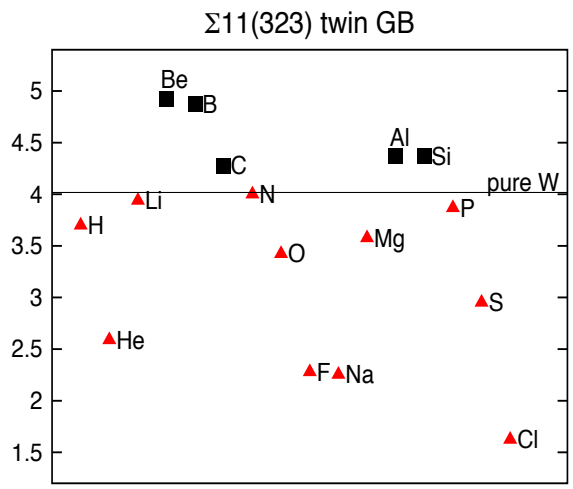

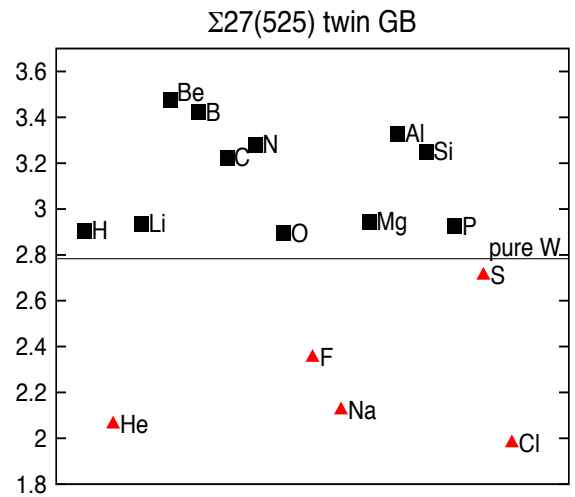

- The nature of covalent bond of Group 3A and 4A elements (B, C, Al, Si) may strengthen tungsten GB cohesion.
- Strengthening effect is stronger for larger-angle GB.

Effect of Substitutional Elements on W Grain Boundary Cohesive Energy

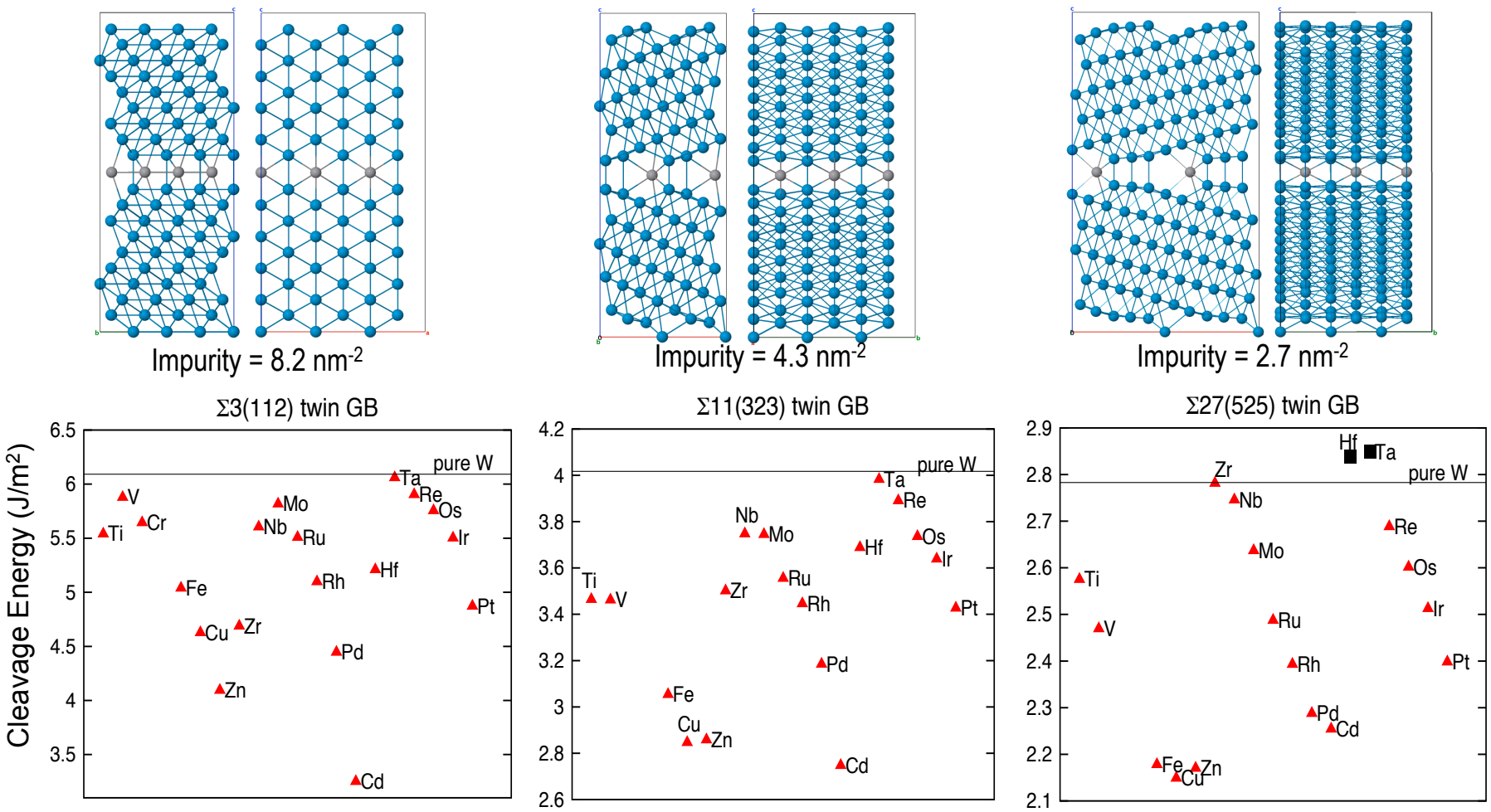

Group 4B and 5B elements (Hf, Ta, Zr, Nb) may strengthen tungsten GB cohesion for large-angle GB.

Interplay of d-Orbital Filling & Cohesive Energy on Tungsten GB Cohesion

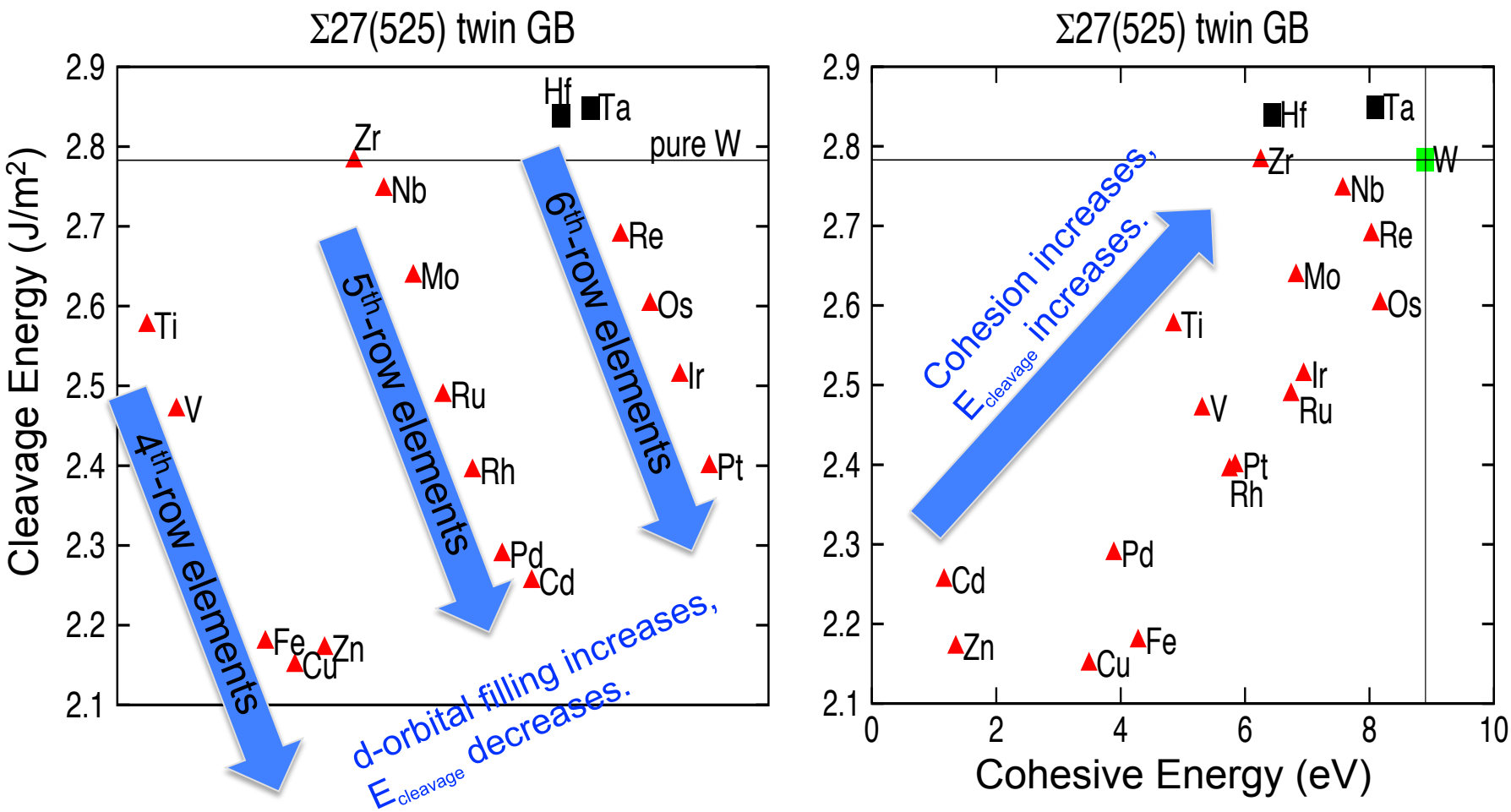

d-orbital occupancy of the 3B, 4B, 5B elements promotes covalent bonding at GB similar to the interstitial case of B, C, Al, Si in increasing GB cohesion.

Multiphysics Simulations of Tungsten Damage.

- A multiphysics model (elastoplasticity + transient heat conduction + helium bubble evolution) is coupled with a damage model that include contact cohesive elements for grain boundary sliding and fracture.

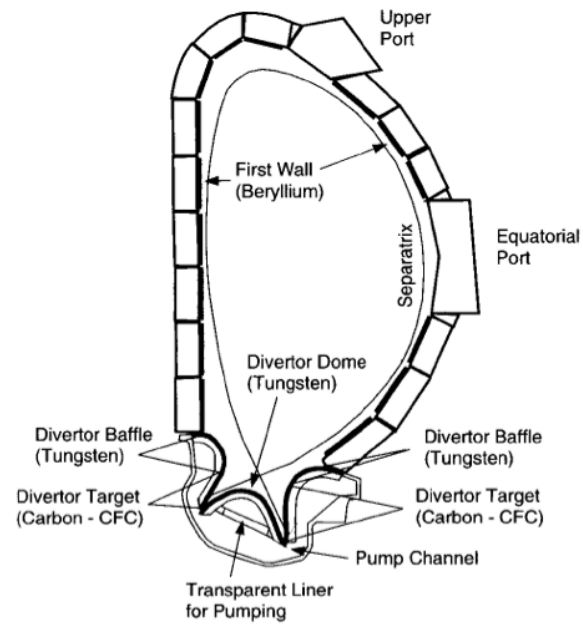

Heat conduction

$$\rho c_p \frac{\partial T}{\partial t} + \nabla \cdot (-k \nabla T) = Q$$

Equilibrium equation

$$\nabla \cdot \boldsymbol{\sigma} + \mathbf{f} = 0$$

Constitutive relation

$$\boldsymbol{\sigma} = \mathbf{C} : \boldsymbol{\epsilon}^e$$

Total strain

$$\boldsymbol{\epsilon} = \boldsymbol{\epsilon}^e + \boldsymbol{\epsilon}^p + \boldsymbol{\epsilon}^\theta, \ \boldsymbol{\epsilon}^\theta = \alpha(T_\infty - T)\mathbf{I}$$

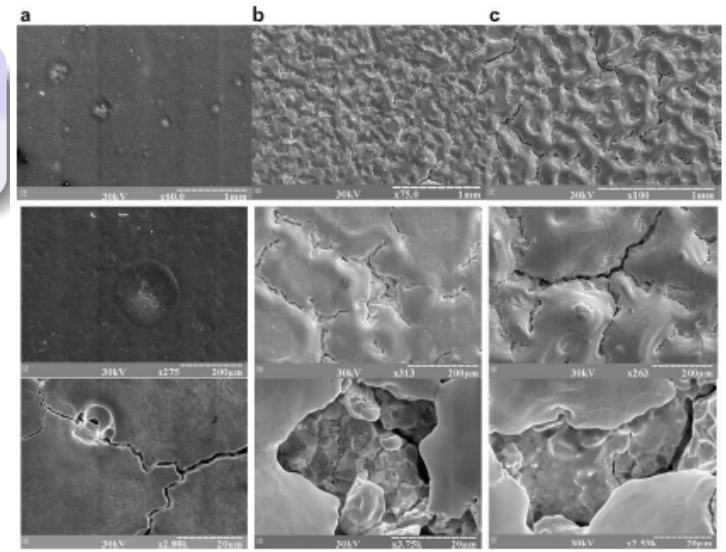

SEM images of tungsten damage, after different number of pulses, Q = 0.75 MJ/m^2. (Garkusha *et. al.* 2009)

- Inward heat flux of 10^4 MW/m^2 is applied for 0.1 ms, on a 10 μm x 10 μm, 2D block, divided into random grains.
- To account for He absorbed on grain boundaries, which leads to crack formation, a body force is applied on the grain boundaries.

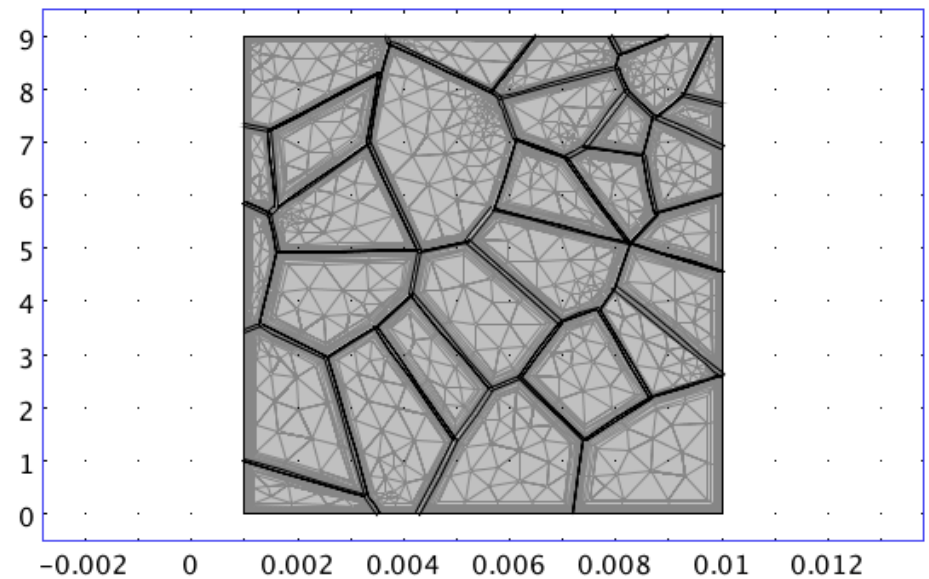

Forces on grain boundaries

$$F = \nabla \cdot (\mathbf{C} : (\epsilon^p + \epsilon^\theta))$$

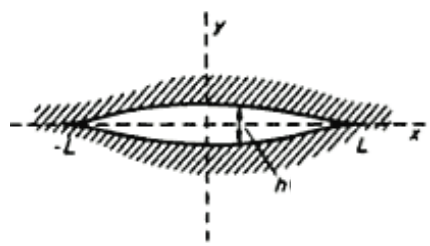

- The model indicates that transient heating of W, already containing He bubbles will result in the evolution of sub-surface residual stresses, material swelling, grain boundary sliding, and subsurface mechanical damage.

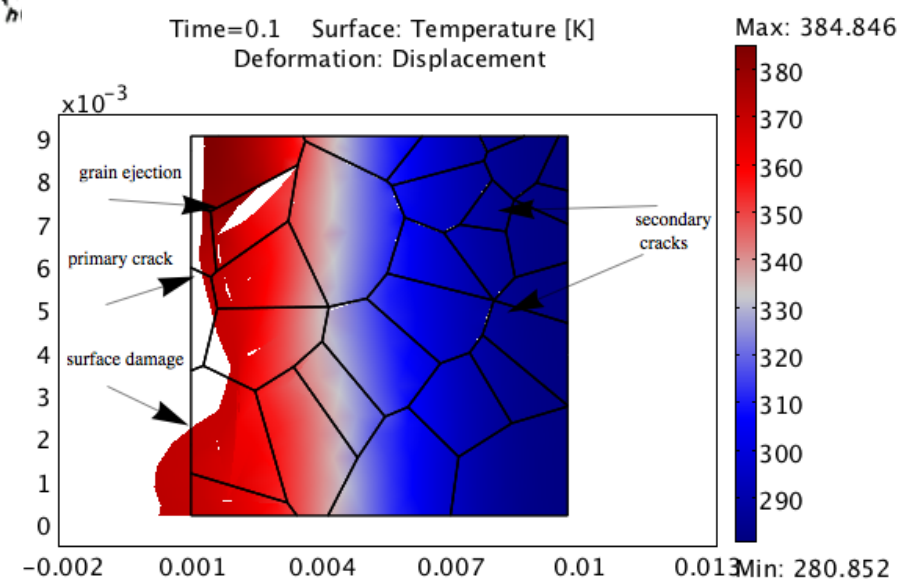

“Textured” tungsten surfaces for mitigation of blistering and thermomechanical damage.

- Radiative heat and implanted plasma ions are distributed into the three-dimensional textured structure, thus changing from a strictly surface to a more volumetric deposition mode.
- Net sputtering erosion due to plasma neutrals is minimized because of geometric trapping of re-deposited atoms within the textured surface.
- Textured surfaces provide a large increase in surface area, promoting better heat distribution and minimizing erosion.
- Thermal stress is reduced and greater ductility is exhibited because fine surface features are capable of a greater level of distortion than a smooth surface.
- The high thermal and dimensional stability of CVD refractory armor prevents fragmentation and dust formation.

Tungsten Micro Nodules

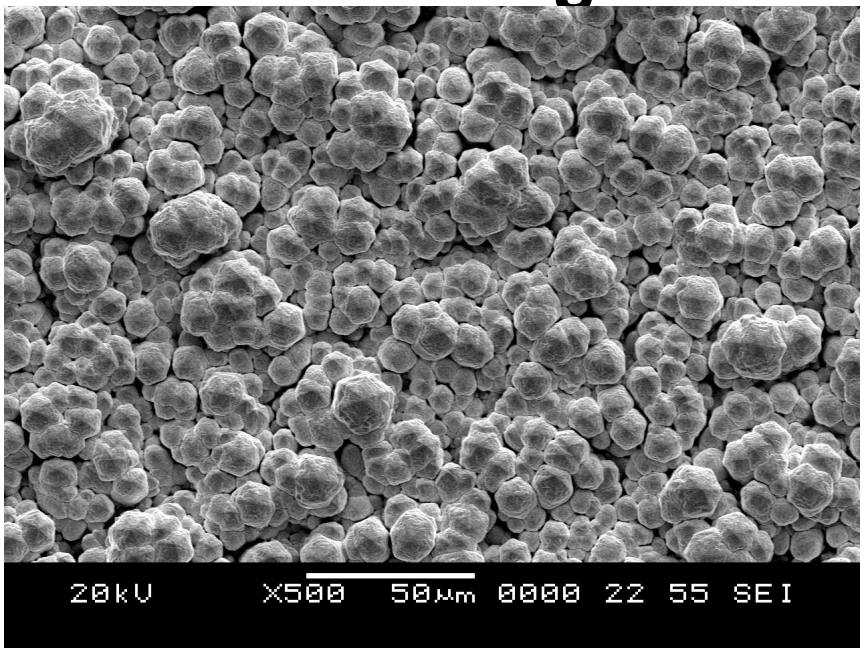

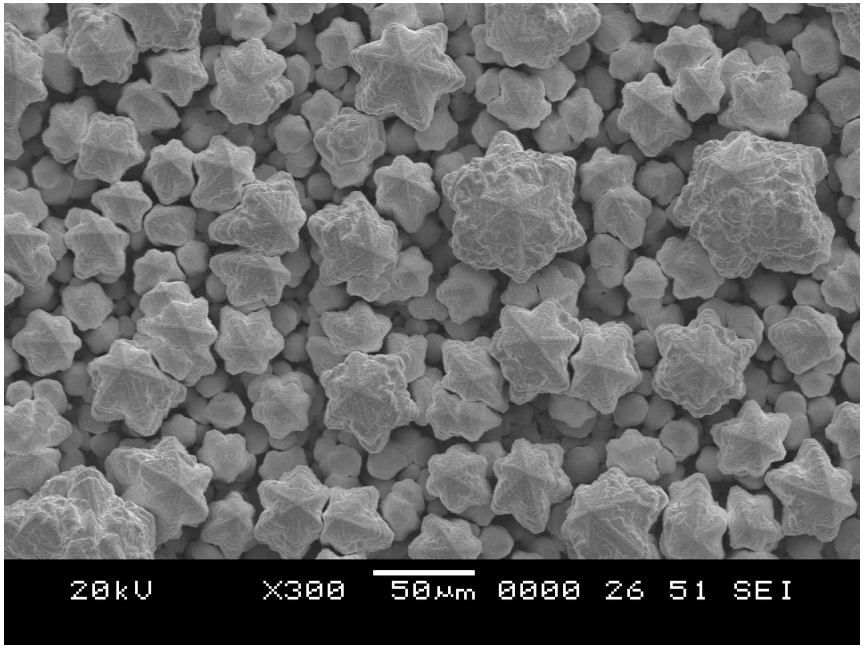

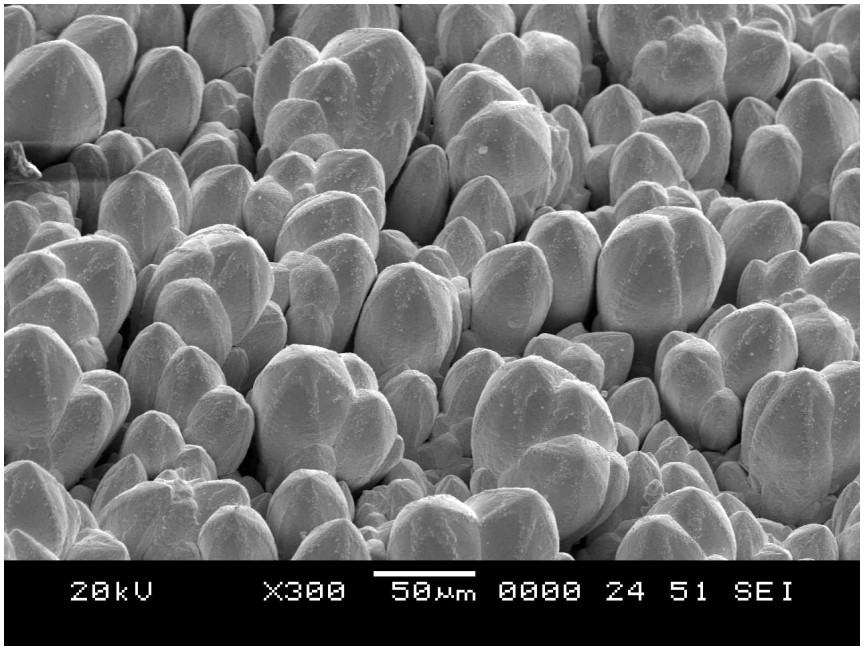

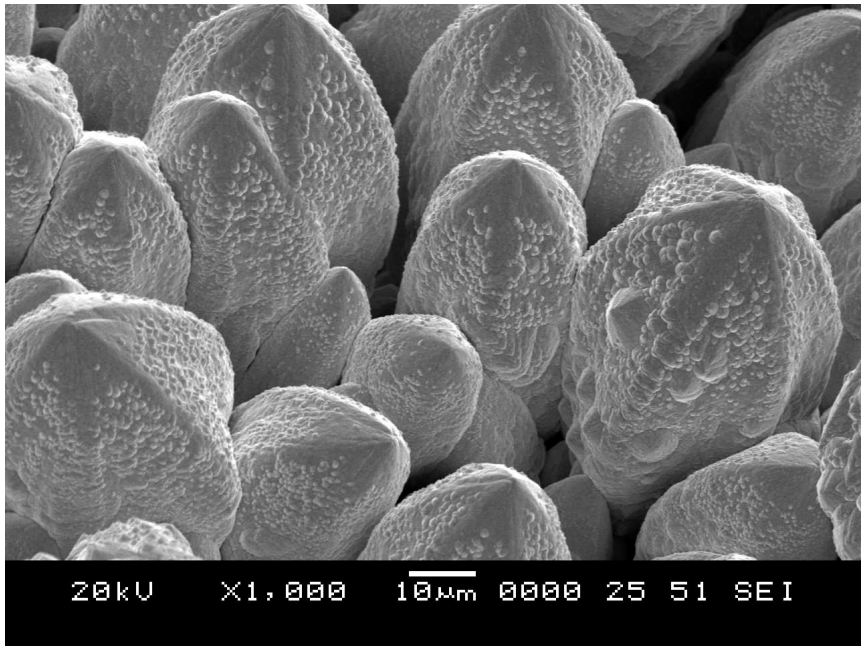

UCLA-McHEROS Code Simulates Surface Pores in W implanted with helium at UW-Madison.

	Temperature (°C)	Implantation Rate (He/cm^2-s)	L_x (μm)	L_y (μm)	L_z (μm)
Model-1	730	2.2x10^{15}	0.2	1.0	1.0
Model-2	990	8.8x10^{15}	0.2	2.5	2.5
Model-3	1160	2.6x10^{16}	0.2	5.0	5.0

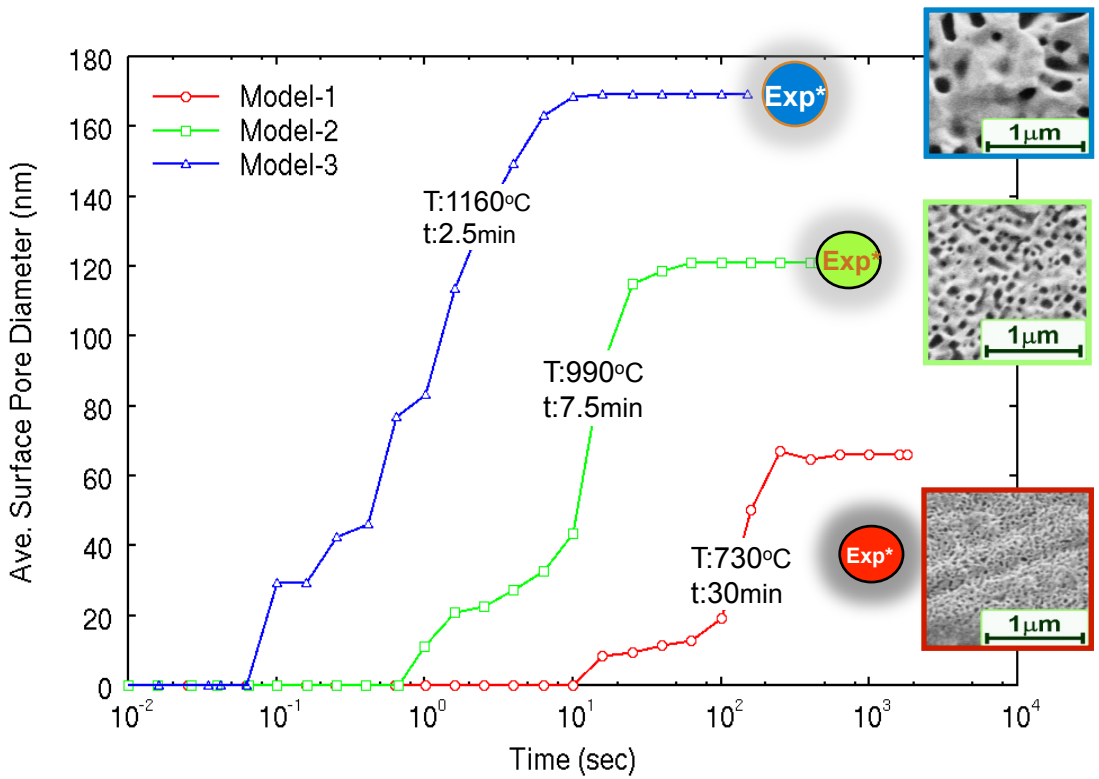

*Exp: IEC (UW-Madison)

2.2x10^{15} He/cm^2-s; 730 °C; t:30min (IEC)

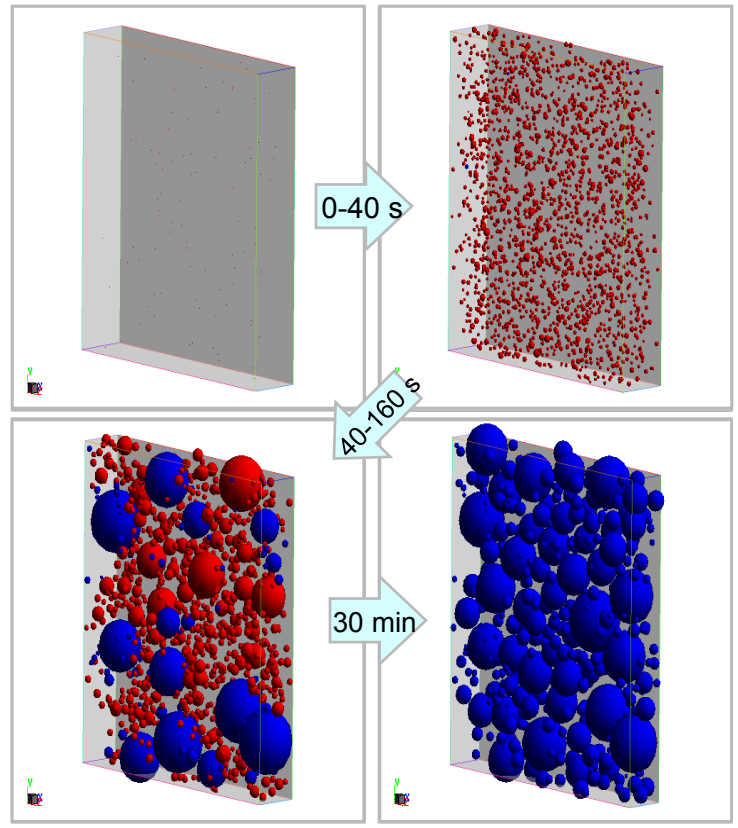

McHEROS Results:

- **Good Agreement between McHEROS Simulation and Experiment**
- **McHEROS provides an *EXPLANATION* for the oversized Surface Pores**